ELSEVIER

Surface Science 423 (1999) 232–242

surface science

Photoemission study of surface state intensity resonance and dispersion of $Be_2C(100)$

C.-T. Tzeng [a], J.-Y. Yuh [b], W.-S. Lo [b], R.-Y. Chu [c], K.-D. Tsuei [b,c,*]

[a] *Institute of Electro-Optical Engineering, National Chiao-Tung University, Hsinchu, Taiwan*
[b] *Synchrotron Radiation Research Center, Hsinchu, Taiwan*
[c] *Department of Physics, National Tsing-Hua University, Hsinchu, Taiwan*

Received 17 November 1998; accepted for publication 30 November 1998

Abstract

We have carried out an extensive study on the surface state properties of an ionic, insulating $Be_2C(100)$ surface using angle-resolved photoemission spectroscopy. Two surface states were observed and characterized. One (S1) is derived at the Γ-point above the valence band maximum in the fundamental gap. The other (S2) is located in the gap at the X-point. Resonance in the photoemission intensity of surface state S2 shows multiple peaks due to a surface umklapp process, similar to bulk transitions, because of large corrugation of the ionic surface. The penetration lengths deduced are about 4 Å for both surface states. The dispersions of these states are very small. These two results indicate strong localization of the surface state wave function to individual surface C atoms owing to the ionic character of this compound. That a surface state (S2) exists in a non-inverted Shockley gap is attributed to the compound structure.

Keywords: Angle-resolved photoemission; Carbides; Insulating films; Surface states; Synchrotron radiation

1. Introduction

The surface state is a fundamental property of a truncated surface. It has been well studied by angle-resolved photoemission from the surfaces of metals, semiconductors, and metallic compounds (for reviews, see S.D. Kevan and W. Eberhardt in chapter 4, G.V. Hansson and R.I.G. Uhrberg in chapter 5, and L.I. Johanson and C.G. Larsson in chapter 6 of Ref. [1]). The localization of a surface state is of high interest and for the simpler sp-derived surface states in metals it has been measured experimentally from resonance in photoemission intensity as a function of photon energy [2–10]. The physics can be understood as follows. A surface state is composed of bulk states of an appropriate $k_{\parallel}$ in the specific bulk bands and it is primarily derived from the bulk state closest in energy to the surface state [2]. The corresponding wave vector perpendicular to the surface can be set as a complex value, $k_{\perp}=K+i\beta$. The real part K is the wave vector where the gap is developed, or the wave vector of the specific bulk state. The imaginary part β indicates that the surface state wave function is confined spatially near the surface and decays exponentially into the bulk. The inverse value $1/\beta$ describes the penetration length of wave function. Thus the photoemission intensity of the surface state should show resonance for photon

* Corresponding author. Fax: +886-3-5789816; e-mail: tsuei@alpha1.srrc.gov.tw.

0039-6028/99/$ – see front matter
PII: S0039-6028(98)00910-8

energies corresponding to the 'direct' transitions from the initial surface state to certain final bulk states. The width of the resonance is related to β and final state broadening [2–9]. The resonance was first successfully analyzed by Louie et al. for the surface states of Cu(111) using a one-dimensional tight-binding (TB) approximation [2]. Later Kevan et al. used a nearly free electron (NFE) model to explain other systems [3–7,9]. The geometrical structure model proposed by Hsieh et al. provides a general description of the resonance behavior [8]. In principle the resonance in photoemission can be calculated directly as done recently [11]. In addition to the resonance measurement the penetration length has also been estimated from the energy splitting of the surface state from the bulk band continuum, [6,7] or determined from the surface state binding energy shift as a function of film thickness [12]. On the other hand, the interpretation of the intensity resonance of d-derived metal surface states is more complicated [5], and whether a resonance occurs in the photoemission intensity of surface states from semiconductor or compound surfaces has largely been ignored.

Recently highly ionic Be_2C thin films with (100) orientation have been successfully synthesized [13]. Unlike transition metal carbides Be_2C has no d electrons and so offers an opportunity to study the compound structure effect on the resonance behavior. We have measured the angle-resolved photoemission spectra from this surface using synchrotron radiation from 18 to 115 eV photon energies. The measured bulk band dispersion is found to be in good agreement with theoretical calculations [14,15]. The result has been published elsewhere [13]. In this paper we focus on the two surface states on this surface. We found that, although this surface is insulating and highly ionic, it is still possible to analyze resonance using the method developed for metals. It was discovered that the ionic compound structure yields many unique properties of the surface states compared with metals, including strong localization to surface atoms, strong surface umklapp process in photoemission [16–19], and the existence of a surface state in a non-inverted Shockley gap.

2. Experiment

Be_2C has the fcc antifluorite structure, which is the same as the calcium fluorite structure, but with the anion and cation interchanged. The C atoms occupy fcc sites and each C atom is surrounded by eight Be atoms at $(\pm 1/4, \pm 1/4, \pm 1/4)a$, where $a = 4.342$ Å is the lattice constant. The structure is similar to the diamond structure but with all tetrahedral sites filled by Be. This compound structure is responsible for the unusual behaviors of bulk photoemission intensity and low energy electron diffraction (LEED) intensity, as described in Appendixes A and B. Not only in its structure but also electronically this compound is isovalent to the group IV elemental semiconductors and to III–V semiconductor compounds.

The experimental procedure and sample preparation have been described in the previous publication. [13] Briefly, thick C_{60} films were evaporated on to a clean Be(0001) surface, and subsequent annealing to 450°C produced a several tens ångstroms thick Be_2C film with three (100) domains rotated by 120° azimuthally. LEED study indicated that (20) and (02) spots appeared around 144 eV kinetic energy; and (10), (01) and (11) spots were very weak and difficult to see. A discussion will be presented in Appendix B. The (100) surface can have either Be or C termination. We did not have a direct method to determine the termination. However, our analysis indicates that both terminations may coexist, as will be discussed later.

3. Results and discussion

3.1. Photoemission spectra and dispersion

Fig. 1(a) shows the valence band normal emission spectra below 9 eV binding energy, with respect to the substrate Fermi level, as a function of photon energy. The dispersive peak P15 is associated with bulk Δ_1 and Δ_5 bands, reaching the critical point Γ_{15} at a photon energy of about 22 eV, which gives the valence band maximum (VBM) at 1.3 eV binding energy. We note here that there is no emission intensity at the Fermi

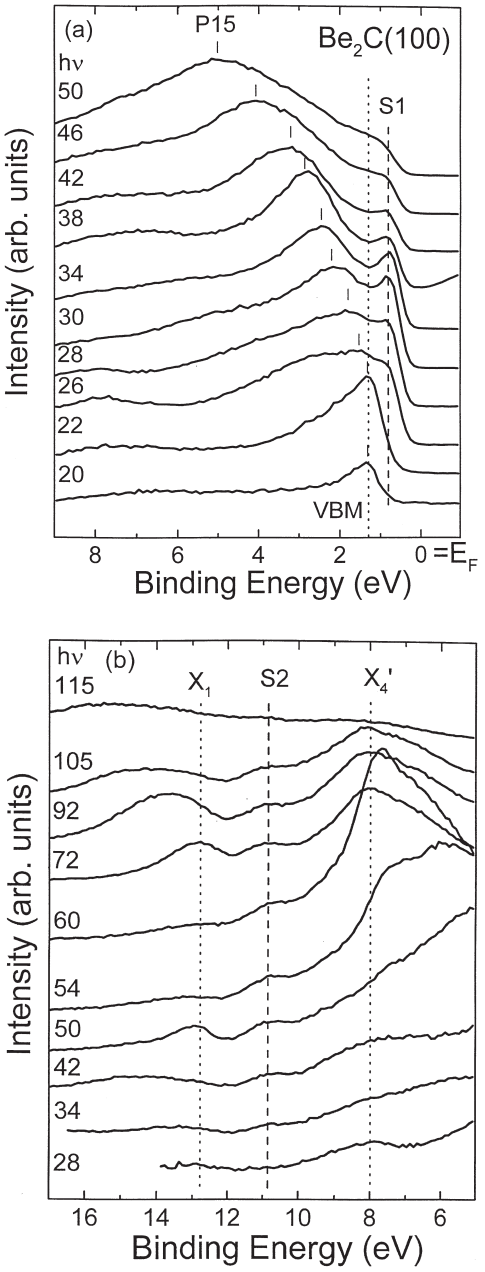

Fig. 1. Normal emission spectra at various photon energies to emphasize (a) surface state S1, and (b) surface state S2. These spectra have been normalized to sample current. The binding energy is referenced to the substrate Fermi level. The dashed lines indicate the surface state peak positions. The dotted lines mark the energy positions of critical points as illustrated. Specifically VBM (Γ_{15}) is at 1.3 eV.

energy, indicating that not only the bulk, but also the surface, is insulating. A non-dispersive peak at 0.8 eV binding energy, above VBM, looks most prominent at around 30 eV photon energy. Its intensity keeps increasing but the line shape overlaps partially with the bulk peak below 30 eV, then decrease quickly below 26 eV. This peak also loses any track above 50 eV. We observed that its intensity attenuated quickly under UHV, presumably being extremely sensitive to surface contamination due to residual gases. Therefore, we identify this peak as a surface state (S1) in the fundamental gap Fig. 1(b) displays another series of normal emission spectra from 5 to 17 eV binding energies at various photon energies. The peak P15 seen in Fig. 1(a) disperses to the critical point X_4' at 8.0 eV binding energy in Fig. 1(b). At higher binding energy the lowest bulk Δ_1 band disperses to a maximum at 12.8 eV binding energy, which marks the critical point of X_1. The non-dispersive peak locates in the band gap at the X-point and is associated with the second surface state (S2). This surface state appears in a much wider photon energy range than S1, from 34 to 113 eV. Compared with S1, S2 is less sensitive to a prolonged exposure to UHV and became more pronounced when more C_{60} was evaporated and annealed. All peaks other than S1 and S2 have been discussed in detail in Ref. [13].

The photoelectron spectra of these two surface states, S1 and S2, at different emission polar angles are presented in Fig. 2(a)and (b), respectively. The full widths at half maximum (FWHM) are about 0.5 eV for S1 and 2.0 eV for S2. The corresponding peak dispersions are plotted in Fig. 3(a) and (b), respectively, as a function of momentum parallel to the surface, $k_{\parallel}=0.512\sqrt{E_k}\sin\theta$. Because of three domains these dispersions should be viewed as an average along $\bar{\Gamma}\bar{M}$ and $+30^{\circ}$. Since the bulk band dispersions along ΓX ($\bar{\Gamma}\bar{M}$) and ΓKX ($\|\bar{\Gamma}\bar{X}$) are not greatly different [14,15], the bulk gap edge at different $k_{\parallel}$ near the surface Brillouin center along these two directions should not be very different. It has been found that the surface state dispersion follows closely the nearest bulk gap edge [20]. As a result we do not expect the surface dispersions would be significantly different along

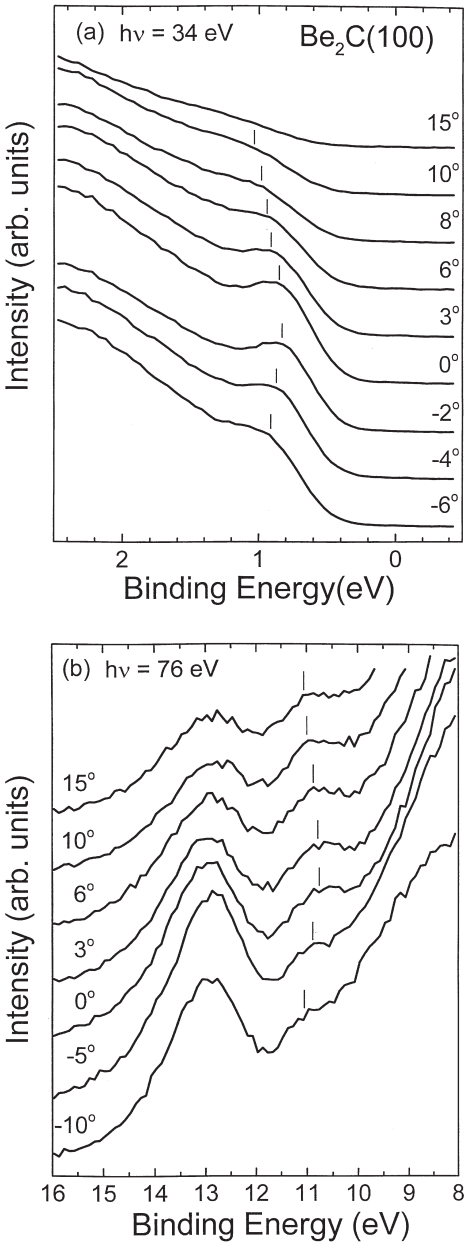

Fig. 2. Photoelectron spectra as a function of emission angles for (a) surface state S1, and (b) surface state S2. The ticks mark the peak positions.

$\bar{\Gamma}\bar{M}$ and $\bar{\Gamma}\bar{X}$. Furthermore, our measured ranges are far from the zone boundaries at $\bar{M}$ (1.45 $Å^{-1}$) and $\bar{X}$ (1.02 $Å^{-1}$); therefore, our measured dispersions resemble fairly the surface state

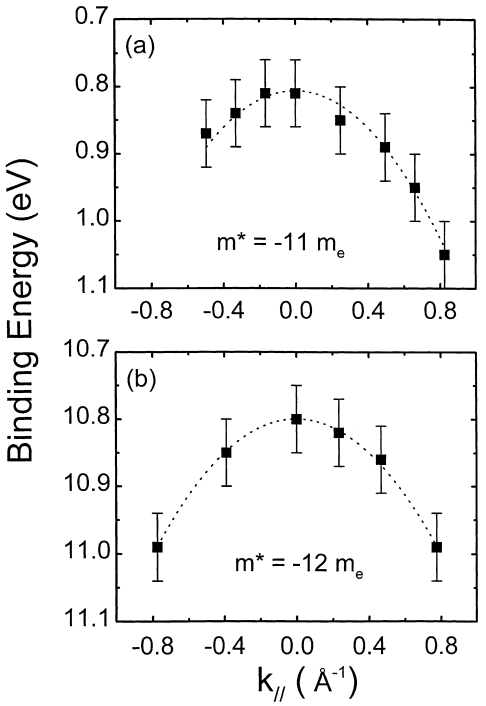

Fig. 3. Peak dispersions of (a) S1, and (b) S2 extracted from Fig. 2. The dotted lines are nearly free electron-like parabolas fitted to the data points and the corresponding effective masses in units of free electron mass m_e are indicated.

dispersion along both directions if measured separately. Experimentally the peak line shape does not degrade significantly away from normal emission, which confirms our prediction. We fit the dispersion curves by parabolas, shown in Fig. 3 as dotted lines, which yield effective masses of $-11m_e$ and $-12m_e$, where m_e is the free electron mass. These large effective masses reflect the small dispersion of these states.

3.2. Intensity resonances and penetration lengths

We review here the geometrical structure model proposed by Hsieh et al. for normal emission [8], and extend it to include the surface umklapp process, as observed experimentally for $Be_2C(100)$. The initial and final state wave functions are of Bloch form

$$\psi_{i,f} = u_{i,f}(\boldsymbol{r}) \exp(i\boldsymbol{k}_{i,f} \cdot \boldsymbol{r}), \quad (1)$$

where $u_{i,f}(\mathbf{r})$ are periodic functions within the crystal. The matrix element

$$M=\langle\psi_f|\boldsymbol{A}\cdot\boldsymbol{P}|\psi_i\rangle \tag{2}$$

can be written as the product of a structure factor and a unit cell form factor. The structure factor is given by

$$S=\sum \exp[i(\boldsymbol{k}_i-\boldsymbol{k}_f)\cdot\boldsymbol{R}], \tag{3}$$

where the summation is over all lattice vectors $\boldsymbol{R}$ in the half-space $x\geq 0$. For the surface state at the surface zone center probed experimentally by a normal-emission geometry, wave vectors of both the initial and final states have zero component in the surface plane. Therefore, $k_i=k_\perp=K+i\beta$ and $k_f=k_{f\perp}$. The result for $|S|^2$ is

$$|S|^2=\{1-2\exp(-\beta x_0)\cos[(k_{f\perp}-K)x_0] +\exp(-2\beta x_0)]\}^{-1}, \tag{4}$$

where x_0 is the interlayer spacing along the x direction. In the case of $Be_2C(100)$ which has an fcc lattice, $x_0=a/2$, where a is the fcc lattice constant. The surface state S2 is derived at the X-point, so that $K=2\pi/a=\Gamma X$. The function $|S|^2$ exhibits peaks at $k_{f\perp}=K$, $3K$, $5K$ etc. as resonances, which has been discussed in Ref. [8]. Physically it means that the resonance occurs when the final state momentum matches the initial state momentum with a reciprocal G vector ($=2K$). For the Γ-point derived surface state S1, $K=4\pi/a$, and the resonance peaks are at $k_{f\perp}=K$, $2K$, $3K$ etc. We note here that the line shape of $|S|^2$ is similar to the sum of Lorentzians with a FWHM of about 2β.

It is interesting to notice that Eq. (4), with $K=\pi/x_0$, is exactly identical to the result from the semi-infinite linear-chain one-band TB model by Louie et al. [2] with the replacement of $\exp(\beta x_0)$ by χ. In the TB model $\chi=4|\Delta/W|>1$, where W is the band width and Δ is the shift in the self-energy of a surface orbital relative to the bulk orbital. The relative amplitude of wave function at adjacent sites is just $-1/\chi$, which has the same physical meaning in the structure model [21,22]. This identity is not very surprising because the structure model treats the unit cell centered at a lattice point individually, similar to the TB model.

For normal emission with a surface umklapp process the final state wave-vector has a component parallel to the surface while the initial state does not, $k_{f\parallel}=G_{f\parallel}$. We need to start from Eq. (3) to obtain a more general form than Eq. (4). The fcc lattice vector can be expressed both in linear combination of primitive cell unit vectors and in Cartesian coordinates, $\boldsymbol{R}=(l, m, n)_p=(m+n, n+l, l+m)(a/2)$. The structure factor becomes

$$S=\sum_{lmn,\ (m+n)\geq 0}\exp[i(K+i\beta-k_{f\perp})(a/2)(m+n)] \times\exp\{-i[k_y(n+l)+k_z(l+m)](a/2)\}, \tag{5}$$

where k_y and k_z are components of final state wave vector parallel to the surface, $k_{f\parallel}$. When $k_y=k_z=0$, Eq. (5) reduces to Eq. (4) with $x_0=a/2$ as it should be. For an umklapp process with G_{002}, $k_{f\parallel}=G'$, Eq. (5) also reduces to Eq. (4). For $G_{1\pm 11}$, $k_{f\parallel}\neq G'$, it produces an extra phase factor $\exp[\pm i(m+n)\pi]$, which gives an additional oscillatory modulation along the x direction. The expression for $|S|^2$ is then

$$|S|^2=\{1+2\exp(-\beta x_0)\cos[(k_{f\perp}-K)x_0] +\exp(-2\beta x_0)\}^{-1}, \tag{6}$$

where $x_0=a/2$. For surface state S2, $K=2\pi/a$; the resonance occurs at $k_{f\perp}=2K$, $4K$, $6K$ etc. The relative intensity of these resonances at different $k_{f\perp}$ or for different umklapp processes depends upon the detailed information from the matrix element, or the unit cell form factor, and will not be explored further.

Fig. 4(a) and (b) displays the intensity profiles as a function of photon energy of S1 and S2, respectively. The intensities of these states were extracted from curve fitting of valence band spectra after subtracting a smooth background. The results are then normalized to total valence band intensity as done in the literature [3–7,9]. This last procedure was found to modify the modulation curve slightly and to improve later line shape analysis. The dotted and dashed lines are fits of data points to Lorentzians centered at transition energies at critical points. For S1, only the data points above 34 eV are used for fitting. The intensity of S1 vanishes below the critical point transition (22 eV) because only one final band is available (Appendix C). Above 22 eV and below 34 eV the data do not

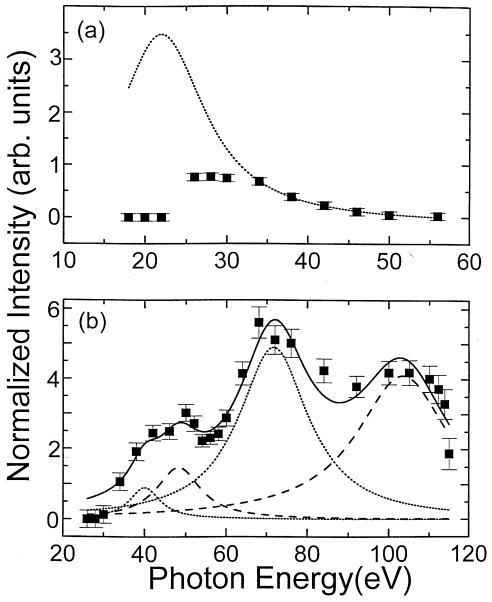

Fig. 4. Surface state intensity (I_S) normalized to total valence band intensity (I_S+I_B) as a function of photon energy for (a) S1, where the dotted line is a Lorentzian fit to the data points above 34 eV centered at the critical point transition energy, and (b) S2, where the dotted and dashed lines are fitted Lorentzians centered at all possible transition energies including surface umklapp process, and the solid line is the sum. See text.

fit to the Lorentzian presumably because the final band deviates from an NFE band. We can still estimate the FWHM to be about 11 eV. The intensity profile of S2 is much more complicated. It spans a range of 80 eV, which is large compared to a nominal value of 20–40 eV for one resonance as seen in the literature. It reveals four features peaked at 41, 49, 72 and 104 eV. These four energies correspond exactly to four sets of final bands around the X-point. Only the main peak at 72 eV corresponds to the ordinary transition to the normal final bands $k+G_{20\pm0}$ and $k+G_{-40\pm0}$, while the other three peaks correspond to surface umklapp transition to the off-normal final bands. These latter final bands are $k+G_{00\pm2}$ and $k+G_{-20\pm2}$ for 41 eV, $k+G_{1\pm1\pm1}$ and $k+G_{-3\pm1\pm1}$ for 49 eV, and $k+G_{20\pm2}$ and $k+G_{-40\pm2}$ for 104 eV peaks, where k is in the $\Gamma\Delta X$ direction and $\Gamma X=(100)(2\pi/a)$. The main peak at 72 eV may have contributions from $k+G_{0\pm2\pm2}$ and $k+G_{-2\pm2\pm2}$ via an umklapp process. It produces no new peaks and is less important than the non-umklapp process.

The true resonance width due to finite surface state wave function penetration can be deduced after subtracting the final state life time broadening, which is discussed in Appendix C. The results are then converted to $k_{f\perp}$ space and displayed in Fig. 5 as dotted and dashed curves. For S1 we approximate the fitted data by a solid curve using Eq. (6) with $1/\beta=4$ Å in Fig. 5(a). For S2 the four peaks in Fig. 4(b) are converted to three peaks in Fig. 5(b). The solid curves are obtained using Eqs. (4) and (6) with $1/\beta=3.8$ Å. The fits are reasonably good. This short penetration length of S2 is consistent with the observation that the surface state energy is near the middle of the gap. One may note that the line shape of $|S|^2$ is symmetric in Fig. 5 while the fitted Lorentzian in k_f space is not. This is because the final state dispersion is

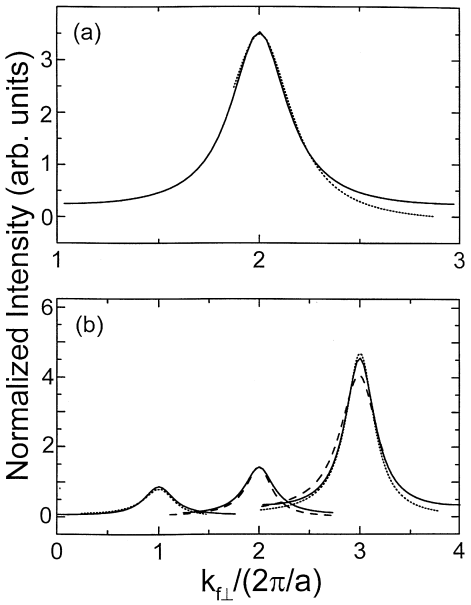

Fig. 5. Surface state resonance in $k_{f\perp}$ space for (a) S1 and (b) S2. The dotted and dashed curves are deduced from the fit in Fig. 4 after subtracting final state broadening. The curves centered at $k_{f\perp}=3(2\pi/a)$ are from peaks at 72 and 104 eV. The curves at $k_{f\perp}=(2\pi/a)$ and $2(2\pi/a)$ are from peaks at 41 and 49 eV, respectively. The solid curve for S1 is calculated from Eq. (4) with $K=4\pi/a$ and $1/\beta=4$ Å. The solid curves for S2 at $k_{f\perp}=(2\pi/a)$ and $3(2\pi/a)$ are from Eq. (4) with $K=2\pi/a$, and at $k_{f\perp}=(2\pi/a)$ from Eq. (6), assuming $1/\beta=3.8$ Å. The relative heights in (b) are the same as the fits in Fig. 4(b).

not linear. In Ref. [8] an expression in k_f space convoluting with final state broadening is derived and it looks symmetric. However, a linear dispersion or constant group velocity is assumed in that derivation. In addition, the tails of $|S|^2$ have contribution from the adjacent peaks so that it always looks higher than the tail of the fitted curve with a Lorentzian line shape. Nevertheless, this minor discrepancy does not affect our conclusion because the uncertainty in the assumption of final state broadening, or mean free path, is comparable with the small difference [3].

We also check the penetration length of S2 by the following formula derived from NFE model [8,23]

$$\epsilon(\beta) = \{[E_g/2 - 2\epsilon(K)]^2 + 4\epsilon(K) - \delta E\}^{1/2} - \delta E + E_g/2 - 2\epsilon(K), \quad (7)$$

where the function $\epsilon(x) = (\hbar x)^2/2m^*$; E_g is the gap energy of 4.8 eV, and $\delta E = 2.0$ eV is the energy splitting of S2 from the lower bulk band in the gap. The effective mass, $m^* \approx 1.5m_e$, is obtained from calculation near bottom of the valence band. [14] The penetration length of S2 thus determined is 3 Å, in agreement with the value obtained from the resonance width previously. Since the gap value at VBM is unknown we choose another formula for S1 valid for small splitting [6,7]

$$\delta E = (\hbar\beta)^2/2|m_{B_\perp}|, \quad (8)$$

where $m_{B_\perp}$ is the effective mass of the lower bulk band. The value of $|m_{B_\perp}|$ is $0.45m_e$ ($0.28m_e$) for Δ_5 (Δ_1) band, obtained from calculation [14]. With $\delta E = 0.5$ eV the penetration length is estimated to be 4 (5) Å, also in agreement with the resonance width.

4. Discussion

The short penetration lengths of these surface states indicate that they are very much localized to the surface layer. The small dispersion suggests minimal overlap of wave functions associated with these surface states between neighboring sites on the surface. Therefore, these two surface states are localized to individual surface atoms. This is due to the strongly ionic bonding character of the crystal as manifested by the calculated valance band charge contour [14], and measured large core level shift [13].

It is interesting to note that the surface state S2 is in the non-inverted gap at the X-point, i.e., $V_G < 0$ [14,15]. Normally there exists a surface state only in an inverted Shockley gap in the two-band, step barrier NFE model [24,25]. The criterion is to match the slope of the wave functions at the surface plane, which is chosen at half the interlattice-plane spacing outside the termination lattice plane. In the structure of $Be_2C(100)$ the lattice planes are composed solely of C atoms and the Be planes are in the middle. The reasonable choice of the surface plane should be at half way between C and Be planes. For a C-terminated surface the surface plane is at one quarter of the interlattice-plane spacing outside the outermost C plane, while for a Be-terminated surface it is at three quarters of the interlattice-plane spacing outside. The slope-matching criterion can be fulfilled at either a C- or a Be-terminated surface. However, since the energy of S2 is closer to the lower bulk band, slope-matching is disfavored at a Be-terminated surface. We noticed that S2 was more pronounced when more C_{60} was deposited and annealed. This is consistent with C termination. On the other hand, S1 appeared at lower film thickness and was more sensitive to residual gas contamination than S2, and is likely to arise from a Be-terminated surface.

We now turn to the orbital properties of these surface states. Since from the calculation there is large charge transfer from Be to C and the whole valence band is largely C derived [14], both surface states consist of atomic-like wave functions centered at C atoms (ions), even though one surface is Be terminated. These surface states may have large C $2p_{yz}$ characters, at least for S1. At the surface zone center both p_y and p_z orbitals are antibonding, while at the zone boundary one is primarily bonding and the other is bonding. Therefore the dispersion is negative. This simple analysis has been applied to explain the dispersion of atomic or molecular adsorbate states on surfaces [26].

Finally we notice that both bulk and surface

state transitions of the $Be_2C(100)$ surface contain a large portion of a surface umklapp process in photoemission, in contrast to metal surfaces. This is because Be_2C is ionic and its surface potential has a large corrugation, which provides the necessary surface G_s vectors for an umklapp process.

5. Conclusion

We found two surface states on $Be_2C(100)$ surfaces in angle-resolved photoemission spectra. The resonance in photoemission intensity of one surface state shows large contribution from a surface umklapp process, owing to its ionic surface. The short penetration length and the small lateral dispersion suggest that these states are very much localized to individual surface C atoms, also consistent with the description of the surface as ionic. That one surface state is in a non-inverted Shockley gap seems anomalous, but can still be understood because the surface plane is different from an elemental crystal; hence matching of the wave function slopes at the surface can be fulfilled. There is evidence that the films had both C-terminated and Be-terminated surfaces, resulting in two surface states.

Acknowledgements

We acknowledge the staff of the SRRC for their technical assistance. One of us (K.D.T) is thankful to J.-L. Chen for providing his calculation of this surface. This work was supported in part by the National Science Council of the ROC.

Appendix A: Bulk photoemission intensity ratio

Bulk photoemission intensity ratio In this appendix we discuss the photoemission cross section of bulk bands. As seen in Fig. 6 of Ref. [13] there are two occupied Δ_1 bands along the ΓX direction around the band gap at the X-point, opened up by the Fourier component of pseudopotential V_{200}. These two bands can be expressed in free electron states $|\boldsymbol{k}\rangle$ and $|\boldsymbol{k}-\boldsymbol{G}_{200}\rangle$, away from the X-point, denoted as lower and upper bands, respectively, in the reduced zone scheme. The direct transition leads to two lowest final bands, $|\boldsymbol{k}+\boldsymbol{G}_{200}\rangle$ and $|\boldsymbol{k}-\boldsymbol{G}_{400}\rangle$ around the X-point at about 70 eV photon energy. Below 70 eV two transitions from the two initial bands to the same final band $|\boldsymbol{k}+\boldsymbol{G}_{200}\rangle$ are energetically allowed, while above 70 eV the final band is $|\boldsymbol{k}-\boldsymbol{G}_{400}\rangle$. In principle, for a given photon energy both initial states can be observed in photoemission. However, as seen in Fig. 5 of Ref. [13], below 70 eV only the upper band is observed, while above 70 eV only the lower band is detected. This transfer of intensity between lower and upper bands has been clearly observed in Al(111) [3], as well as, to a lesser degree, in Al(100) [10]. The major difference between the two Al cases and ours is that in the former, across the critical point transition, the intensity transfer is from the lower to upper bands. A model focused on the hybridization of free electron bands near the zone boundary has been proposed to explain the intensity transfer in the Al cases [3]. Here we present an alternative interpretation focusing on regions away from the zone boundary, where hybridization is negligible, to explain our, as well as previous, observations.

The intensity variation can be understood as follows. The photoemission intensity may be expressed as

$$I \propto |\langle \mathrm{f}|\nabla V|\mathrm{i}\rangle|^2, \tag{A1}$$

where $V(\boldsymbol{r})=\Sigma_G V_G \exp(\mathrm{i}\boldsymbol{G}\cdot\boldsymbol{r})$ is the Fourier expansion of the pseudopotential. For a given transition we obtain

$$I \propto |GV_G|^2, \tag{A2}$$

and $\boldsymbol{G}=\boldsymbol{k}_\mathrm{f}-\boldsymbol{k}_\mathrm{i}$. Specifically below 70 eV the intensity ratio between upper and lower bands for $Be_2C(100)$ is

$$\frac{I_\mathrm{u}}{I_\mathrm{l}} \propto \frac{|G_{400}V_{400}|^2}{|G_{200}V_{200}|^2} = 4\left|\frac{V_{400}}{V_{200}}\right|^2. \tag{A3}$$

Above 70 eV the ratio $I_\mathrm{u}/I_\mathrm{l}$ becomes reversed. Therefore, the intensity transfer is an intrinsic property of the crystal coupled to the photoemission process. Usually for a crystal with only one atom at the fcc site, $V_{400} \ll V_{200}$. However, Be_2C is

a compound; there are three atoms per unit cell: one carbon atom at the fcc site and two Be atoms at $\pm\boldsymbol{u}$, where $\boldsymbol{u}=(1/4,1/4,1/4)a$. We can write, following Ref. [27]

$$V(\boldsymbol{G})=(1/\Omega_{\text{cell}})\int_{\text{cell}} V(\boldsymbol{r})\exp(-\mathrm{i}\boldsymbol{G}\cdot\boldsymbol{r})\,\mathrm{d}^3r, \qquad \text{(A4)}$$

where Ω_{cell} is the volume of the unit cell. Writing $\boldsymbol{G}=(h,k,l)\ 2\pi/a$, we have

$$\begin{aligned} V(\boldsymbol{G}) &= (1/\Omega_{\text{cell}})\{\Omega_{\text{C}}V^{\text{C}}(\boldsymbol{G}) \\ &\quad + 2\Omega_{\text{Be}}V^{\text{Be}}(\boldsymbol{G})\cos[(\pi/2)(h+k+l)]\} \\ &= V_1(\boldsymbol{G})+V_2(\boldsymbol{G})\cos[(\pi/2)(h+k+l)], \qquad \text{(A5)} \end{aligned}$$

where Ω_{C} and Ω_{Be} are the atomic volumes of C and Be, respectively; $V^{\text{C}}(\boldsymbol{G})$ and $V^{\text{Be}}(\boldsymbol{G})$ are the corresponding pseudopotentials; and V_1 and V_2 are the associated form factors. Using this expression we obtain $V_{200}=V_1-V_2$, while $V_{400}=V_1+V_2$. If V_1 and V_2 contribute out of phase to V_{200}, while in phase with V_{400}, the resulting ratio $4|V_{400}/V_{200}|^2$ could become greater than unity. The actual values of V_1 and V_2 at G_{200} and G_{400} for Be_2C are not known. However, these values for Mg_2Si, also with antifluorite structure, have the same sign; and the ratio $4|V_{400}/V_{200}|^2$ is greater than unity [27]. We expect the same case for Be_2C. This explains our observation of intensity transfer. The large V_{400} may be anticipated directly from the antifluorite crystal structure. When viewed along the [100] direction the lateral C and Be planes appear alternately with a distance of $a/4$, thus the value of V_{400} becomes enhanced. On the other hand, Al has only one atom per unit cell and the most relevant Fourier components of pseudopotential are V_{111} and V_{200}; the corresponding $2G$ components V_{222} and V_{400} are rather small. Thus the intensity ratios, $4|V_{400}/V_{200}|^2$ for Al(100) and $4|V_{222}/V_{111}|^2$ for Al(111) surfaces, are less than unity, opposite to the case of $Be_2C(100)$, as experimentally observed.

Appendix B: Intensity of LEED

We explain in this appendix why we observed only (20) spots at around 144 eV kinetic energy,

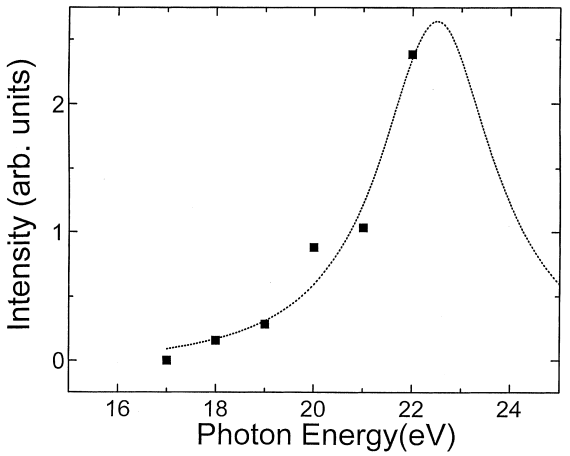

Fig. 6. Photoemission intensity of bulk transition at Γ_{15} (VBM) at photon energies below 22 eV. The dotted line is the fit to a Lorentzian with a FWHM of 2.9 eV

and the (10) and (11) spots were almost invisible. Only three-dimensional single-scattering, kinematic theory will be addressed to give a qualitative account. The diffraction amplitude is the product of the structure and the unit cell form factor. The structure factor $S(\boldsymbol{k}_{\text{f}}-\boldsymbol{k}_{\text{i}})=S(\boldsymbol{Q})=\sum_{\boldsymbol{R}}\exp[\mathrm{i}\boldsymbol{Q}\cdot\boldsymbol{R}]$, where it sums up all lattice points $\boldsymbol{R}$, defines the diffraction condition, $\boldsymbol{Q}=\boldsymbol{G}$. In surface, due to short electron mean free path, the diffraction relaxes to $\boldsymbol{Q}_{\parallel}=\boldsymbol{G}_{\text{s}}=\boldsymbol{G}_{\parallel}$, but the intensity peak still follows primarily $\boldsymbol{Q}_{\perp}=\boldsymbol{G}_{\perp}$ [28]. Under such conditions the unit cell form factor becomes $F(\boldsymbol{G})=\Sigma_j A_j(\boldsymbol{G})\exp[\mathrm{i}\boldsymbol{G}\cdot\boldsymbol{r}_j]$, where it sums up all atoms j in a unit cell; A_j and $\boldsymbol{r}_j$ are the atomic form factor and position relative to the lattice site, respectively, of atom j. The unit cell form factor modulates the amplitude of diffraction spots if there is more than one atom per unit cell. The evaluation of $F(\boldsymbol{G})$ is similar to $V(\boldsymbol{G})$ described in the previous section. However, we choose here one C atom at an fcc site and eight Be atoms at $\boldsymbol{u}=(\pm1/4,\ \pm1/4,\ \pm1/4)a$, with 1/4 contribution from each Be atom, in order to preserve the $Be_2C(100)$ surface symmetry. The results indicate that for (10) spots the unit cell form factor has contribution only from the C atom, $F=A_{\text{C}}$. The relevant G's are (511), (711) and (911), etc. For (20) spots the relevant G's are (622) and (822) with F equal to $A_{\text{C}}-2A_{\text{Be}}$ and $A_{\text{C}}+2A_{\text{Be}}$, respec-

tively. For (11) spots the relevant G's are (602) and (802) with F equal to A_C+2A_{Be} and A_C-2A_{Be}, respectively. These G's are chosen to have kinetic energy less than 200 eV and within our LEED geometric condition. We may approximate the atomic form factors between Z and Z/G [29], where Z is the total number of electrons associated with the atom at the given site, and the charge state can be assumed between neutral and completely ionic. It is found that the only relevant (20) spot occurs around 162 eV (822), which is not far from the experimental value of 144 eV; and the only relevant (11) and (10) spots are around 89 (602) and 58 eV (511), respectively. We actually found very faint spots between 50 and 80 eV, consistent with this simple analysis. We emphasize here that the unusual behavior of photoemission intensity transfer and LEED intensity is largely due to the compound structure resulting in enhancement or cancellation effect on the pseudopotential or unit cell form factor.

Appendix C: Final state life time broadening

The final state life time broadening, or the mean free path of final state electrons was an unknown factor in deducing the surface state penetration length from the resonance line shape. Usually 5–7 Å was assumed from the universal curve [3,6,7,9]. In the case of Be_2C we can measure the final state broadening for a given energy directly from our photoemission data. As seen in Fig. 1, the intensity of surface state S1 virtually vanishes below 22 eV photon energy, leaving only the bulk transition at VBM (Γ_{15}) with identical line shape but continuously decreasing intensity. We plot in Fig. 6 the bulk photoemission intensity around VBM as a function of photon energy below 22 eV. The data points can well be fitted by a half-Lorentzian centered at 22.5 eV, which is the experimentally determined transition energy right at the Γ-point, with a FWHM of 2.9 eV. This behavior can be understood if there exists a large band gap and no final band is available for transition below 22.5 eV. The decrease in intensity is because of the transition to the tail of final state due to life time broadening, which is represented by the fitted FWHM. This behavior is different from the X critical point, which has been discussed in Appendix A.

This width of 2.9 eV represents the life time broadening of a final electron state with an energy around 22 eV above VBM. If we use the free electron band approximation the corresponding electron mean free path is 7.6 Å, which is a reasonable value. We further assume that the mean free path does not change in the range of surface state resonance. Then the life time width is proportional to the final momentum. For bulk Be the measured life time broadening is about 3 eV at 21 eV and 4 eV at 92 eV final states, in good agreement with our result [30].

References

[1] S.D. Kevan (Ed.), Angle-Resolved Photoemission, Elsevier, Amsterdam, 1992.
[2] S.G. Louie, P. Thiry, R. Pinchaux, Y. Petroff, D. Chandesris, J. Lecante, Phys. Rev. Lett. 44 (1980) 549.
[3] S.D. Kevan, N.G. Stoffel, N.V. Smith, Phys. Rev. B 31 (1985) 1788.
[4] S.D. Kevan, N.G. Stoffel, N.V. Smith, Phys. Rev. B 31 (1985) 3348.
[5] S.D. Kevan, N.G. Stoffel, N.V. Smith, Phys. Rev. B 32 (1985) 4956.
[6] S.D. Kevan, R.H. Gaylord, Phys. Rev. Lett. 57 (1986) 2975.
[7] S.D. Kevan, R.H. Gaylord, Surf. Sci. 178 (1986) 229.
[8] T.C. Hsieh, P. John, T. Miller, T.-C. Chiang, Phys. Rev. B 35 (1987) 3728.
[9] S.D. Kevan, R.H. Gaylord, Phys. Rev. B 36 (1987) 5809.
[10] H.J. Levinson, F. Greuter, E.W. Plummer, Phys. Rev. B 27 (1983) 727.
[11] S.-K. Ma, K.W.-K. Shung, Phys. Rev. B 49 (1994) 10617.
[12] T.C. Hsieh, T. Miller, T.-C. Chiang, Phys. Rev. Lett. 55 (1985) 2483.
[13] C.-T. Tzeng, K.-D. Tsuei, W.-S. Lo, Phys. Rev. B 58 (1998) 6837.
[14] J.L. Corkill, M.L. Cohen, Phys. Rev. B 48 (1993) 17138.
[15] C.H. Lee, W.R.L. Lambrecht, B. Segall, Phys. Rev. B 51 (1995) 10392.
[16] G.D. Mahan, Phys. Rev. B 2 (1970) 4334.
[17] T.-C. Chiang, J.A. Knapp, M. Aono, D.E. Eastman, Phys. Rev. B 21 (1980) 3513.
[18] T.-C. Chiang, R. Ludeke, M. Aono, G. Landgren, F.J. Himpsel, D.E. Eastman, Phys. Rev. B 27 (1983) 4770.
[19] B.S. Itchkawitz, I.-W. Lyo, E.W. Plummer, Phys. Rev. B 41 (1990) 8075.
[20] F.J. Himpsel, D.E. Eastman, Phys. Rev. Lett. 41 (1978) 507 for example.

[21] E.T. Goodwin, Proc. Camb. Philos. Soc. 35 (1939) 221.
[22] M.C. Desjonqueres, D. Spaniaard, Concepts in Surface Physics, 2nd Ed., Springer-Verlag, Berlin, 1996, p. 224.
[23] N.V. Smith, Phys. Rev. B 32 (1985) 3549.
[24] E.T. Goodwin, Proc. Camb. Philos. Soc. 35 (1939) 205.
[25] A.W. Maue, Z. Phys. 94 (1935) 717.
[26] W. Eberhardt, E.W. Plummer, Adv. Chem. Phys. 49 (1982) 533 for example.
[27] M.Y. Au-Yang, M.L. Cohen, Phys. Rev. 178 (1969) 1358.
[28] J.B. Pendry, Low Energy Electron Diffraction, Academic Press, New York, 1974. (Chapter 3).
[29] C. Kittel, 5th Ed. Wiley, New York, 1976. (Chapter 2).
[30] E. Jensen, R.A. Bartynski, T. Gustafsson, E.W. Plummer, M.Y. Chou, M.L. Cohen, G.B. Hoflund, Phys. Rev. B 30 (1984) 5500.